Magnetic resonance angiography: From anatomical knowledge modeling to vessel segmentation

Nicolas Passat, Christian Ronse, Joseph Baruthio, Jean-Paul Armspach, Claude Maillot

Magnetic Resonance Angiography: From Anatomical Knowledge Modeling to Vessel Segmentation

N. Passat [a,b,*], C. Ronse [a], J. Baruthio [b], J.-P. Armspach [b], C. Maillot [c]

[a] *LSIIT, UMR 7005 CNRS-ULP (Laboratoire des Sciences de l'Image, de l'Informatique et de la Télédétection), Bd S. Brant, BP 10413, F-67412 Illkirch Cedex, France*

[b] *IPB-LNV, UMR 7004 CNRS-ULP (Institut de Physique Biologique - Laboratoire de Neuroimagerie in Vivo), Faculté de Médecine, 4 rue Kirschleger F-67085 Strasbourg Cedex, France*

[c] *Institut d'Anatomie Normale, Faculté de Médecine, 4 rue Kirschleger F-67085 Strasbourg Cedex, France*

Abstract

Magnetic resonance angiography (MRA) has become a common way to study cerebral vascular structures. Indeed, it enables to obtain information on flowing blood in a totally non-invasive and non-irradiant fashion. MRA exams are generally performed for three main applications: detection of vascular pathologies, neurosurgery planning, and vascular landmark detection for brain functional analysis. This large field of applications justifies the necessity to provide efficient vessel segmentation tools. Several methods have been proposed during the last fifteen years. However, the obtained results are still not fully satisfying. A solution to improve brain vessel segmentation from MRA data could consist in integrating high-level a priori knowledge in the segmentation process. A preliminary attempt to integrate such knowledge is proposed here. It is composed of two methods devoted to phase contrast MRA (PC MRA) data. The first method is a cerebral vascular atlas creation process, composed of three steps: knowledge extraction, registration, and data fusion. Knowledge extraction is performed using a vessel size determination algorithm based on skeletonization, while a topology preserving non-rigid registration method is used to fuse the information into the atlas. The second method is a segmentation process involving adaptive sets of gray-level hit-or-miss operators. It uses anatomical knowledge modeled by the cerebral vascular atlas to adapt the parameters of these operators (number, size, and orientation) to the searched vascular structures. These two methods have been tested by creating an atlas from a 18 MRA database, and by using it to segment 30 MRA images, comparing the results to those obtained from a region-growing segmentation method.

Key words: anatomical knowledge modeling, brain vessel segmentation, magnetic resonance angiography, mathematical morphology.

1 Introduction

Vessel segmentation and quantification from 3D cerebral angiographic images has become an important field of research in medical image processing. Indeed, the availability of accurate information concerning brain vessels is fundamental not only for planning and performing neurosurgery procedures, but also for diagnosing vascular pathologies such as aneurysms or stenoses. Recent research works (functional imaging, magnetic transcranial stimulation) have also emphasized the role of vessels as landmarks for localization of brain specific areas.

Although computed tomography angiography (CTA) remains the most accurate way to generate 3D vascular images, magnetic resonance angiography [1] (MRA) has become a commonly used acquisition process. Indeed MRA enables to obtain flowing blood images without radiation or contrast agent injection. Two different non-invasive MRA techniques have been developed: time of flight MRA [2] (TOF MRA) and phase-contrast MRA [3] (PC MRA).

The advantages of 3D MRA acquisition coupled with the necessity to obtain reliable information from angiographic data has led to the development of several vessel segmentation methods during the last fifteen years. Nearly all of them are based on an intensive use of classical image processing tools. However, although the majority of these concepts have been studied and applied for vessel segmentation purpose, the obtained results are still not fully satisfactory. In order to improve the efficiency of vessel segmentation methods, an original approach could consist in integrating high-level a priori anatomical knowledge in segmentation strategies. This knowledge could then be used to guide image processing tools during the segmentation.

Such a knowledge-based approach however generates several issues: what knowledge can be used, how this knowledge can be modeled and how it can be integrated in a segmentation algorithm. In this paper, a solution composed of two methods is proposed. The first method enables to model high-level anatomical knowledge (vascular density, vessel size, and vessel orientation,) into a cerebral vascular atlas. The second method uses this atlas to guide mathematical morphology tools (gray-level hit-or-miss operators) in a vessel segmentation process. Both methods are designed for PC MRA data, taking advantage of the bi-modality (magnitude and phase images) of this acquisition technique (Fig. 1).

The paper is organized as follows. In Section 2, a general overview of the main strategies devoted to vessel segmentation from MRA is proposed. In Section 3, the way to model anatomical knowledge concerning vessels by use of atlases is discussed. Section 4 provides definitions and notations used in the paper. In Section 5, the first method, enabling to generate a cerebral vascular atlas from a database,

* Corresponding author: Nicolas Passat (passat@dpt-info.u-strasbg.fr).

is detailed. In Section 6, the second method using such an atlas to guide gray-level hit-or-miss operators during a vessel segmentation process is fully described. In Section 7, both methods are validated on a 48 PC MRA database, 18 images being used for atlas generation while the 30 other ones are used to evaluate the accuracy of the segmentation process. Discussion on possible applications of vascular atlases and on knowledge-based vessel segmentation methodology are presented in Section 8.

2 Previous work on vessel segmentation

Vessel segmentation is an active research area since 1990, already providing a large amount of methods for 2D, multi-planar 2D, and 3D angiographic data. Several publications presenting overviews of all vessel segmentation methods or of segmentation algorithms devoted to specific angiographic images are available in the literature [4–7]. In this section, we will only focus on methods devoted to vessel segmentation from 3D MRA data.

2.1 Segmentation methods

Several criteria could be used to classify vessel segmentation methods: automation, centerline or whole vessel detection, size of the searched vessels, general methods or methods designed for a specific organ. The classification proposed here is based on the main image processing strategies used to carry out the segmentation. According to this taxonomy, eight categories, being presented hereafter, can be considered: filtering, mathematical morphology, region-growing, vessel tracking, differential analysis, deformable models, statistical analysis, and artificial intelligence.

Filtering methods have constituted the very first algorithms used for analysis of MRA data [8]. In [9], it is proposed to use anisotropic diffusion to reduce the signal to noise ratio without blurring the object boundaries. In [10], the dispersion range of low-pass filters in the 13 main directions of a cubical neighborhood is used to enhance the visibility of small vessels. The line segment model used in this method is generalized to a cylinder of finite width in [11]. In [12], anisotropic filtering is also carried out by previously determining the orientation of the vessels, finally proposing a nonlinear approach. In more recent works, local structure estimation is carried out as a preliminary step using six 3D selective filters in [13], while computation of the local maximum mean is proposed in [14] to enhance vessel visualization in maximum intensity projections (MIP) of MRA. It has to be noticed that other methods involving multi-resolution filtering are classified as differential analysis methods, since they use filters based on Hessian matrix analysis.

Mathematical morphology is an image processing framework designed for analysis of signals in terms of shape. Many classical mathematical morphology tools have been used in the field of MRA segmentation. Hysteresis thresholding is performed in [15] as a preliminary step before analyzing the vascular network topology. More recently, sophisticated concepts have also been involved in segmentation methods. Indeed, watershed is used for segmentation of specific venous structures in [16] and as a preliminary step in [17] before classifying the different connected component into vessels or non vascular structures. Segmentation by gray-scale skeletonization is also used in [18] to segment vascular structures containing subvoxel-sized vessels. It has to be noticed that many other tools have also been applied for vessel segmentation from CTA (gray-level opening and closing, thinning, ...).

Region-growing methods are based on the hypothesis that vessels can be reconstructed from a seed point by iteratively adding voxels belonging to the vascular network. This approach is used in [19,20] to improve MIP visualizations of vessels, and in [21] to improve vein/artery discrimination. In [22], region-growing segmentation is used for creation of 3D models for neurosurgery planning. A similar method is also proposed in [23] for visualization purpose. The seed point used to initialize the segmentation method is generally interactively defined by the user or chosen according to an intensity criterion. The growing process is then carried out according to given connectivity criteria and a threshold value indicating when the method has to finish.

Vessel tracking methods are generally designed to segment the axis and boundary of a vessel from an interactively defined initial point. Following an iterative process, the method determines a vessel slice before computing the following slice center along the vessel axis and the normal plane at the new position. This process, behaving as an imaginary catheter is useful for segmentation and quantification of vessels in case of pathology diagnosis. Such a strategy is proposed in [24], where the point assumed to be located on the axis is determined by computing a center likelihood measure. In [25], the whole vascular tree is segmented by recursively applying the tracking method on each new detected branch. A method proposed in [26] also enables a detection of whole vascular trees by using an adaptive box surrounding the processed area to detect topology modifications.

Differential analysis methods are designed to segment vascular structures by computing differential properties of the 3D data which are then considered as functions. Following preliminary results proposed in [27], several methods are based on multi-scale filtering using Hessian matrix analysis. In [28] the proposed method uses a combination of eigenvalues of the Hessian matrix while both eigenvalues and eigenvectors are considered in [29] to characterize vascular structures. Strategies presenting similarities are proposed in [30] and [31,32]. They consider the 3D data as hypersurfaces in a 4D space and segment vessels as crest lines of such surfaces.

Deformable models are used in vessel segmentation methods in order to determine vessel axes or vessel walls. These models are designed to evolve under external and internal constraints such as vessel shape and intensity criteria. A level-set approach is proposed in [33] to segment vessel axes before estimating their radius. In [34] a vessel model, using axial position and circumference parameters, is used as a deformable model, assuming that the searched vessel present a circular cross-section. In [35], a surface mesh which must present a correct topology in the region of interest is deformed to fit the vessel walls in this region. It has to be noticed that deformable models can be mixed with other segmentation strategies as in [36] where Hessian matrix analysis is used to guide a B-spline curve deformation.

Statistical analysis methods are designed to find vascular structures by using different statistical distributions to model both flowing blood and background signals. An expectation-maximization algorithm is generally used to classify each voxel of the processed angiographic image. In [37], a Maxwell-Gaussian mixture density is used to model the background signal distribution while a uniform distribution is used for blood signal in PC MRA data. In [38], TOF MRA are processed by using a mixture of one Rayleigh and two normal distributions for background, and a normal distribution for vessels. In [39], classification is performed in a hierarchical way, to adapt the model to the different subvolumes of the processed TOF MRA.

Several artificial intelligence concepts have also been applied to the field of vessel segmentation. The major part of vessel segmentation methods using artificial intelligence are path finding techniques enabling to determine the trajectory of a vessel from two given extremity points, even in case of signal loss caused by vascular pathologies. Although most of them are devoted to CTA segmentation, applications on MRA have also been proposed in [40]. Other artificial intelligence concepts have been studied. A classification based on neural networks is then proposed in [41] to segment vessels from non vascular structures.

2.2 Analysis

Despite a large amount of methods, one can observe that very few strategies have been developed to take advantage of anatomical knowledge. The assumption that vessels present a circular cross-section has been used in [34] for vessel modeling in a deformable model method. Topology information is sometime provided by vessel segmentation methods as in [42]. However, topology is never used to guide the segmentation process, except in [43], where the tree structure of the searched vascular network is used for guidance of a thinning process. Such hypotheses on vascular structure anatomy, which could enable to create knowledge-based methods remain very infrequent, hence forbidding to obtain strategies adapting their behavior to the processed structures.

One can also observe that multimodal data are generally not involved in vessel segmentation processes. In [44], a method using both 3D MRA and 2D X-ray images, is proposed for brain vessel visualization, taking advantage of the accuracy of X-ray data and of the 3D information provided by MRA. In [45], another multimodal approach is proposed for reconstruction of 3D vascular data from 2D X-ray images and ultrasound data. Except such examples, this kind of method remains unusual. Moreover, the few methods using multimodal data only consider angiographic images, while integration of non angiographic ones could provide useful information, as shown in [16].

In the following section, the use of multimodal (angiographic and non angiographic) images and of a priori anatomical knowledge is discussed. It is then observed that both concepts can be used to build anatomical knowledge models leading to the proposal of new kinds of knowledge-based vessel segmentation methods.

3 Anatomical knowledge modeling

3.1 Vascular knowledge

All the vessel segmentation methods presented in the previous section use very little a priori knowledge. Indeed, they are generally based on two main hypotheses. First, vessels (*i.e.* flowing blood) correspond to the voxels of highest value in MRA, justifying the use of threshold-based strategies. Second, vessels present a tubular shape (*i.e.* a circular or elliptic cross-section). This hypothesis is generally used to guide deformable model evolution. It also enables to propose methods based on medial axis detection such as vessel tracking or path-finding ones. Few methods also use topological properties, assuming that vascular networks, or parts of them, are generally organized in a tree structure.

Nevertheless, brain vascular networks present many other important properties concerning density [1] , size, orientation, and adjacency with other structures. All these properties may allow to create vascular models of brain vasculature designed to guide segmentation tools. The way to model such knowledge by use of atlases is now discussed.

3.2 Vascular atlases

Atlases modeling knowledge properties of n-D structures are generally defined as n-D images. Therefore, they provide an easy and efficient way to store informa-

[1] "Density" is defined here as the probability to find a vessel at a given position.

tion according to spatial position. 3D atlases are then perfectly designed to model knowledge concerning anatomical structures. Such atlases have already been proposed for segmentation of cerebral non angiographic data [46]. Nevertheless, the tortuosity and variability of brain vessels make the creation of vascular atlases a hard task. Despite these difficulties, two attempts have recently been proposed.

In [47,48], a process is proposed to generate vascular atlases from any database of segmented angiographic images. For each segmented image, an inverted distance map is computed, providing a blurred image of the vasculature. An arbitrary element of the database being defined as the reference template, the other ones are then mapped on it, using affine registration (directly based on the distance maps or on T2 MRI associated to MRA). Both mean and variance images obtained by fusing the registered images finally constitute the vascular atlas.

In [49], the proposed atlas is designed from a PC MRA magnitude image (similar to a classical T1 MRI), using semi-automated segmentation tools. Its main purpose is to provide a set of regions presenting homogeneous properties about vessel size, orientation and position relative to other brain structures. This atlas is then used for guidance of region-growing segmentation from PC MRA phase images.

To our knowledge, these two results constitute the very first attempts to model anatomical information on cerebral vascular structures. Despite their originality, both of them present drawbacks. The first atlases are automatically generated by directly registering segmented vessels [47] and by using affine transform [47,48]. Then the atlas generation process can hardly take into account the anatomy of the neighboring cerebral structures, and may be inaccurate and error prone. Although this strategy enables to generate atlases for any vascular structures (it has been applied for brain arterial structures and liver vessels), such atlases are not designed for segmentation purpose. The second atlas described in [49] is devoted to segmentation and takes into account information concerning the vessels in relation with other cerebral structures. Despite these advantages, it has not been automatically generated, and can contain imperfections. It also has to be noticed that it divides the brain into a finite set of vascular areas. This finite number of regions could be considered as a weakness, since there is no automated process to determine new smaller regions from the initial ones.

The method proposed in Section 5 for cerebral vascular atlas generation, has been developed to avoid these drawbacks. Indeed, it is designed to automatically generate atlases which are not composed of regions, but model knowledge as vector fields. Moreover, vascular knowledge is fused by using non-rigid registration, allowing a better precision than affine registration. Finally, registration is not performed on angiographic images (PC MRA phase images) but on non vascular images associated to them (PC MRA magnitude images). This use of multimodal data enables to preserve the relation between the vessels and the neighboring cerebral structures.

4 Background

4.1 Imaging

The proposed methods have been designed to be performed on PC MRA. A PC MRA data is composed of two 3D images: a magnitude image, similar to a T1 MRI, and a phase image, only containing moving structure signal (flowing blood, plus noise and artifacts). Both images are simultaneously acquired and are then perfectly superimposed. Sagittal slices of PC MRA magnitude and phase images are illustrated in Fig. 1. These images are generally made of non-isotropic voxels of edges equal or close to 1 mm. A MRA image of the whole head can then be composed of more than 150 slices, each one containing 256^2 voxels.

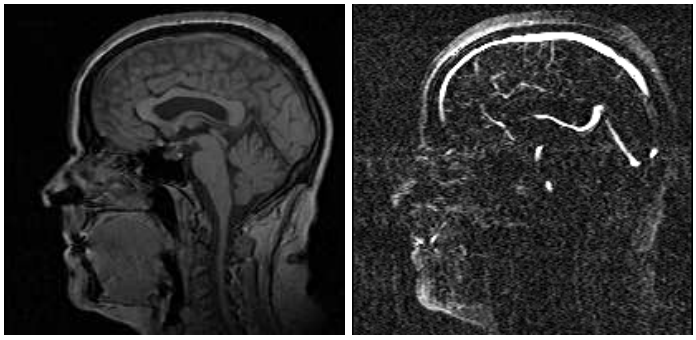

Fig. 1. PC MRA sagittal slices. Left: magnitude image (p_{mag}) slice, containing morphological structures. Right: phase image (p_{pha}) slice visualizing the flowing blood. By definition, both images are perfectly superimposed.

4.2 Definitions and notations

In the following, a PC MRA data will be denoted by p while a set of PC MRA's will be denoted by P. The magnitude image (resp. phase image) associated to p will then be denoted by p_{mag} (resp. p_{pha}). Since phase and magnitude images of p are 3D gray-level images, they can be defined as functions. Then, if d_x, d_y, d_z are the dimensions of p, we have:

$$\left| \begin{array}{ccc} p_\alpha : [0, d_x - 1] \times [0, d_y - 1] \times [0, d_z - 1] & \to & \mathbb{Z} \\ (x, y, z) & \mapsto & v \end{array} \right. ,$$

where $\alpha = mag$ or pha and v is the gray-level value of the image at the current point (x, y, z). For simplicity's sake, we will consider that for a given set P, all $p \in P$ have

the same dimensions d_x, d_y, d_z. The set $[0, d_x - 1] \times [0, d_y - 1] \times [0, d_z - 1]$ will be denoted by I while a point $(x, y, z) \in I$ will be denoted by $\mathbf{x}$.

The following definitions and notations will be used in the sequel ($\mathcal{E}$ is a Euclidean or digital space):

- $\mathcal{P}(X)$ – set of all subsets of X: $\forall X \subseteq \mathcal{E}, \mathcal{P}(X) = \{Y \mid Y \subseteq X\}$;
- X^c – complementary of X: $\forall X \subseteq \mathcal{E}, X^c = \{x \in \mathcal{E} \mid x \notin X\}$;
- X_p – translation of X by p: $\forall X \subseteq \mathcal{E}, \forall p \in \mathcal{E}, X_p = \{x + p \mid x \in X\}$;
- $\check{X}$ – symmetric of X: $\forall X \subseteq \mathcal{E}, \check{X} = \{-x \mid x \in X\}$;
- $\overline{\mathbb{R}}^{\mathcal{E}}$ – set of numerical functions $F : \mathcal{E} \to \overline{\mathbb{R}}$ ($\overline{\mathbb{R}} = \mathbb{R} \cup \{-\infty, +\infty\}$);
- F^* – dual function of F: $\forall F \in \overline{\mathbb{R}}^{\mathcal{E}}, \forall x \in \mathcal{E}, F^*(x) = -F(-x)$;
- F_p – translation of F by p: $\forall F \in \overline{\mathbb{R}}^{\mathcal{E}}, \forall p \in \mathcal{E}, \forall x \in \mathcal{E}, F_p(x) = F(x - p)$;
- $F_{(p,t)}$ – translation of F by (p, t): $\forall F \in \overline{\mathbb{R}}^{\mathcal{E}}, \forall (p, t) \in \mathcal{E} \times \mathbb{R}, \forall x \in \mathcal{E}, F_{(p,t)}(x) = F(x - p) + t$;
- $\bigvee_{F \in \mathcal{F}}$ – supremum of $\mathcal{F}$: for all $\mathcal{F} \subseteq \overline{\mathbb{R}}^{\mathcal{E}}, \forall x \in \mathcal{E}, (\bigvee_{F \in \mathcal{F}})(x) = \sup_{F \in \mathcal{F}}(F(x))$;
- $\bigwedge_{F \in \mathcal{F}}$ – infimum of $\mathcal{F}$: for all $\mathcal{F} \subseteq \overline{\mathbb{R}}^{\mathcal{E}}, \forall x \in \mathcal{E}, (\bigwedge_{F \in \mathcal{F}})(x) = \inf_{F \in \mathcal{F}}(F(x))$;
- $U(F)$ – umbra of F: $\forall F \in \overline{\mathbb{R}}^{\mathcal{E}}, U(F) = \{(p, t) \in \mathcal{E} \times \mathbb{R} \mid t \leq F(p)\}$;
- $F \oplus B$ – dilation of F by B: $\forall F \in \overline{\mathbb{R}}^{\mathcal{E}}, \forall B \in \mathcal{P}(\mathcal{E}), F \oplus B = \sup_{b \in B} F_b$;
- $F \ominus B$ – erosion of F by B: $\forall F \in \overline{\mathbb{R}}^{\mathcal{E}}, \forall B \in \mathcal{P}(\mathcal{E}), F \ominus B = \inf_{b \in B} F_{-b}$;
- $F \oplus G$ – dilation of F by G: $\forall F, G \in \overline{\mathbb{R}}^{\mathcal{E}}, F \oplus G = \bigvee_{(p,t) \in U(G)} F_{(p,t)}$;
- $F \ominus G$ – erosion of F by G: $\forall F, G \in \overline{\mathbb{R}}^{\mathcal{E}}, F \ominus G = \bigwedge_{(p,t) \in U(G)} F_{(-p,-t)}$.

5 Vascular atlas generation

The method described in this section has been designed to generate vascular atlases from any set of PC MRA's of the brain. The obtained atlases model anatomical knowledge on vessel size and orientation but also on vascular density, with respect to the position of cerebral non vascular structures.

5.1 Input and output

The method takes as input a PC MRA database $P = \{p^i\}_{i=0}^{n-1}$ of arbitrary size n and a PC MRA magnitude image p^{ref}_{mag} used as a reference image (p^{ref}_{mag} can be chosen in P). It provides as output a vascular atlas $\mathcal{A}$ defined by:

$$\left| \begin{array}{l} \mathcal{A} : I \to [0,1] \times \mathcal{P}(\mathbb{R}^+) \times \mathcal{P}([0, \pi[\times[0, \pi[) \\ \qquad \mathbf{x} \mapsto (\mathcal{A}^d(\mathbf{x}), \mathcal{A}^t(\mathbf{x}), \mathcal{A}^o(\mathbf{x})) = (d, t, o) \end{array} \right. ,$$

where (d, t, o) represents the vascular density (d), the set of possible diameters of a vessel (t), and the set of its possible orientations (o) at the current position $\mathbf{x}$.

5.2 First step: Knowledge extraction

This first step consists in determining anatomical information for each MRA of the database. Information about vessel position is first obtained by segmentation. Information on vessel orientation and size is then determined using a quantitative analysis method.

The vessel segmentation method takes as input $P = \{p^i\}_{i=0}^{n-1}$ and computes the segmentation of p^i for $i = 0$ to $n - 1$. The method used here [49] is based on a region-growing algorithm, the results of which are then interactively corrected to provide correct and accurate segmentations [2]. However, any method providing a discrete binary image as result could also be used. Each segmentation of p^i provides a 3D binary image p^i_{seg} containing the arterial and venous structures contained in p^i:

$$\left| \begin{array}{l} p^i_{seg} : I \rightarrow \{0, 1\} \\ \qquad \mathbf{x} \mapsto \quad d \end{array} \right. ,$$

where $d = 1$ if a vessel is located at $\mathbf{x}$, and 0 otherwise. A new set $P_{seg} = \{p^i_{seg}\}_{i=0}^{n-1}$ of segmented images associated to P is then available. A segmented image example is illustrated in the left picture of Fig. 3.

The set P_{seg} can be used to compute the probability of finding a vascular structure at a given position. Nevertheless, it does not directly provide information on vessel size and orientation. A quantitative analysis is then necessary to complete the knowledge extraction step. In order to compute size and orientation parameters, every binary image p^i_{seg} is processed by a quantitative evaluation method fully described in [50]. This quantitative evaluation is first based on an iterative topology preserving skeletonization of the binary image. At each iteration, only simple voxels [51] (voxels whose deletion does not modify the object topology) are considered and deleted from p^i_{seg}. The final skeleton, obtained by successive layers removal, has the same topology as the vessels and is centered inside each of them, but can however present an irregular shape. Since a direct estimation of the tangent lines from this skeleton could then lead to incorrect results, each branch is modeled by a Bézier curve. The control points used for each curve are determined by sampling the skeleton (*i.e.* by choosing points separated by a fixed number of voxels on the

[2] These corrections constitute the only interactive part of the method. This interaction is however necessary since, to our knowledge, there does not exist any vessel segmentation method being fully automatic and fully reliable.

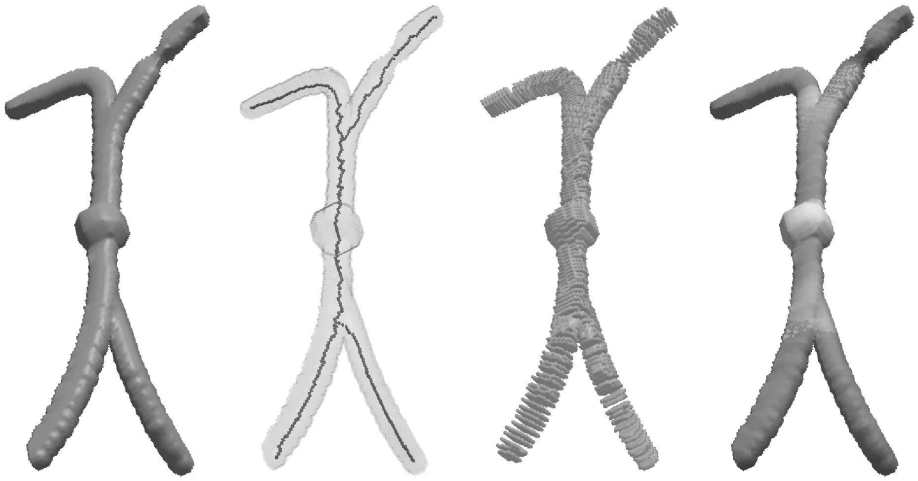

Fig. 2. Successive steps of the quantitative estimation method applied on a virtual object. From left to right: initial object; skeleton computation; cross-section planes computed by intersecting the object and the digital normal planes; thickness image obtained from area estimation (the gray-level depends on the estimated diameter of the cross-section planes).

discrete curve corresponding to the branch). The use of Bézier curves enables to significantly smooth the skeletal structure, finally providing reliable medial axes being correctly oriented and centered in the object. It is then possible to efficiently determine the tangent line corresponding to the vessels axes, and hence to define an image p^i_{ske}, which is composed of their orientations. Tangent lines also enable to determine digital planes being normal to the vessel axes. The intersection of both normal plane and vessel provides a model of the vessel cross-section for each point of the skeleton. Each cross-section can be directly projected onto the three principal planes, providing three areas A_x, A_y, and A_z which can be combined with the normal vector (n_x, n_y, n_z) associated to the tangent line to compute the cross-section area:

$$A = A_x.n_x + A_y.n_y + A_z.n_z.$$

Assuming that cross-section planes present a circular or nearly circular shape, the diameter can be directly evaluated from the area value, enabling to compute an image p^i_{thi} modeling these diameters. The different steps of the quantitative analysis method are illustrated on a simple shape example in Fig. 2.

That step finally provides, for every $p^i \in P$, two 3D images p^i_{thi} and p^i_{ske}:

$$\left| \begin{array}{rcl} p^i_{thi} : I & \rightarrow & \mathbb{R}^+ \\ \mathbf{x} & \mapsto & t \end{array} \right. ,$$

$$\left| \begin{array}{ll} p^i_{ske} : I \rightarrow & [0,\pi[\times[0,\pi[\\ \mathbf{x} \mapsto & (p^i_{ske,\theta}(\mathbf{x}), p^i_{ske,\phi}(\mathbf{x})) = o \end{array} \right. ,$$

where $p^i_{thi}(\mathbf{x}) = t$ (resp. $p^i_{ske}(\mathbf{x}) = o$) is the diameter (resp. the 3D orientation) of the vessel in the neighborhood of $\mathbf{x}$ ($p^i_{thi}(\mathbf{x})$ and $p^i_{ske}(\mathbf{x})$ are defined if and only if $p^i_{seg}(\mathbf{x}) \neq 0$). It has to be noticed that θ represents the angular position of the vessel with respect to the vertical axis (where $\theta = 0$), while ϕ is the angular position of the vessel with respect to the sagittal axis (where $\phi = 0$). After this quantitative analysis, two new sets $P_{thi} = \{p^i_{thi}\}_{i=0}^{n-1}$ and $P_{ske} = \{p^i_{ske}\}_{i=0}^{n-1}$ of diameter and orientation images associated to P are available. Examples of skeleton and diameter images are respectively illustrated in the middle and right parts of Fig. 3.

Fig. 3. 3D visualization of the computed parameters for an image p^i of the database P. From left to right: segmented vessels (p^i_{seg}), skeleton (p^i_{ske}), vessel diameter (p^i_{thi}: gray-level depending on the vessel diameter).

5.3 Second step: Non-rigid registration

In order to correctly combine the information of every image of the database, it is necessary that the fused values correspond to the same position in the brain or the head. Indeed, even though the principal parts of the human brain are quite similar from one person to another, their size, shape and proportions can present variations. It is then fundamental to find, for every processed image, a correct 3D deformation field enabling to map them on a same reference. This can be done by use of non-rigid registration. The registration algorithm used here (illustrated in Fig. 4) is the one proposed in [52,53]. It relies on a hierarchical parametric modeling based on B-spline functions. The parameters of the model are estimated by minimizing a symmetric form of the standard sum of squared differences criterion. This method has been chosen for its ability to preserve the topology of the registered anatomical structures by constraining the Jacobian of the transformation to remain positive.

For all $p^i \in P$, the PC MRA magnitude image p^i_{mag} is registered onto the reference

magnitude image p^{ref}_{mag}, providing a 3D deformation field D^i. Then for any $\mathbf{x} \in I$, $p^i(\mathbf{x})$ is assumed to be equal to $p^{ref}_{mag}(D^i(\mathbf{x}))$, from an anatomical point of view.

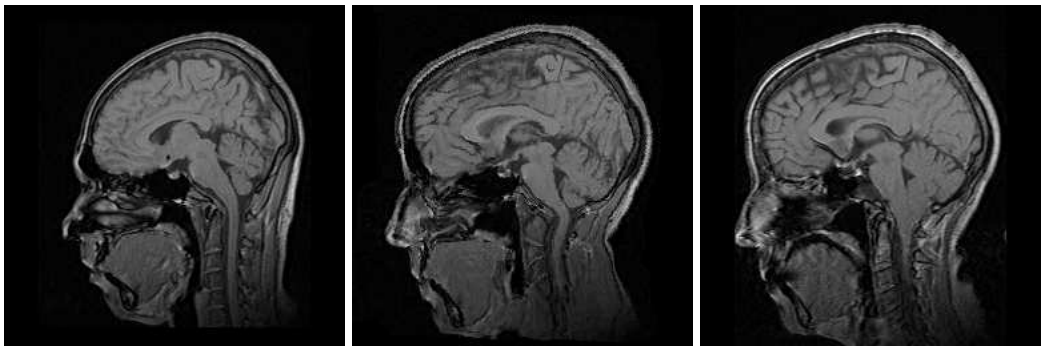

Fig. 4. Result provided by the 3D non-rigid registration used in the proposed algorithm. Left: reference magnitude image (p^{ref}_{mag}). Right: magnitude image of a patient case (p^i_{mag}). Middle: result obtained by registration of the left image on the right image. The deformation field used here to obtain this image (D^i) is then used to map the atlas on the phase image of the patient.

5.4 Third step: Data fusion

This last step consists in fusing the pieces of knowledge of each image of the database into a unique vascular atlas. The first part of the atlas (modeling vascular density information):

$$\left| \begin{array}{rcl} \mathcal{A}^d : I & \rightarrow & [0,1] \\ \mathbf{x} & \mapsto & d \end{array} \right. ,$$

is defined from the set P_{seg}, by computing the average image of all $p^i_{seg} \in P_{seg}$:

$$\forall \mathbf{x} \in I, \mathcal{A}^d(\mathbf{x}) = \frac{1}{n} \sum_{i=0}^{n-1} p^i_{seg}((D^i)^{-1}(\mathbf{x})).$$

By definition, $\mathcal{A}^d(\mathbf{x}) \in [0,1]$, and provides the probability to find a vascular structure at the current position $\mathbf{x}$ of p^{ref}_{mag}.

The second part of the atlas (modeling vessel size information):

$$\left| \begin{array}{rcl} \mathcal{A}^t : I & \rightarrow & \mathcal{P}(\mathbb{R}^+) \\ \mathbf{x} & \mapsto & t \end{array} \right. ,$$

is defined using average and standard deviation diameter values obtained from all $p^i_{thi} \in P_{thi}$:

$$\forall \mathbf{x} \in I, \mathcal{A}^t(\mathbf{x}) = [\max\{0, a(\mathbf{x}) - \sigma_a(\mathbf{x})\}, a(\mathbf{x}) + \sigma_a(\mathbf{x})],$$

where:

$$a(\mathbf{x}) = \begin{cases} 0 & \text{if } N(\mathbf{x}) = \emptyset \\ \frac{1}{\#N(\mathbf{x})} \sum_{i \in N(\mathbf{x})} p^i_{thi}((D^i)^{-1}(\mathbf{x})) & \text{otherwise} \end{cases},$$

with:

$$N(\mathbf{x}) = \{i \in [0, n-1] \mid p^i_{seg}((D^i)^{-1}(\mathbf{x})) = 1\},$$

$\#X$ standing for the cardinal of a set X, and $\sigma_a(\mathbf{x})$ standing for the standard deviation associated to $a(\mathbf{x})$. This definition, using the standard deviation and the average value of the vessel diameters, enables to take into account their variability between the different cases.

The last part of the atlas (modeling vessel orientation information):

$$\left| \begin{array}{ccc} \mathcal{A}^o : I & \to & \mathcal{P}([0,\pi[\times[0,\pi[) \\ \mathbf{x} & \mapsto & o \end{array} \right. ,$$

is defined by using the 3D orientation data provided by P_{ske} to generate a set of possible orientations:

$$\forall \mathbf{x} \in I, \mathcal{A}^o(\mathbf{x}) = \Theta(\mathbf{x}) \times \Phi(\mathbf{x}),$$

where:

$$\Theta(\mathbf{x}) = \begin{cases} \emptyset & \text{if } N(\mathbf{x}) = \emptyset \\ [0, \pi[& \text{if } N(\mathbf{x}) \neq \emptyset \text{ and } \sigma_\theta(\mathbf{x}) \geq \pi/4 \\ [\theta(\mathbf{x}) - \sigma_\theta(\mathbf{x}), \theta(\mathbf{x}) + \sigma_\theta(\mathbf{x})] \pmod{\pi} & \text{otherwise} \end{cases},$$

$$\Phi(\mathbf{x}) = \begin{cases} \emptyset & \text{if } N(\mathbf{x}) = \emptyset \\ [0, \pi[& \text{if } N(\mathbf{x}) \neq \emptyset \text{ and } \sigma_\phi(\mathbf{x}) \geq \pi/4 \\ [\phi(\mathbf{x}) - \sigma_\phi(\mathbf{x}), \phi(\mathbf{x}) + \sigma_\phi(\mathbf{x})] \pmod{\pi} & \text{otherwise} \end{cases},$$

with:

$$\theta(\mathbf{x}) = \sum_{i \in N(\mathbf{x})} \frac{1}{\#N(\mathbf{x})} p^i_{ske,\theta}((D^i)^{-1}(\mathbf{x})),$$

$$\phi(\mathbf{x}) = \sum_{i \in N(\mathbf{x})} \frac{1}{\#N(\mathbf{x})} p^i_{ske,\phi}((D^i)^{-1}(\mathbf{x})),$$

and $\sigma_\theta(\mathbf{x})$ (resp. $\sigma_\phi(\mathbf{x})$) standing for the standard deviation associated to $\theta(\mathbf{x})$ (resp. $\phi(\mathbf{x})$). It has been chosen to set $\Theta(\mathbf{x})$ (resp. $\Phi(\mathbf{x})$) to $[0, \pi[$, *i.e.* its maximum size, if the standard deviation was higher than $\pi/4$. Indeed, in such cases, one can consider that there is no significant vessel orientation at the position $\mathbf{x}$.

The three parts, $\mathcal{A}^d$, $\mathcal{A}^t$, and $\mathcal{A}^o$ finally provide the whole atlas $\mathcal{A}$. It has to be noticed that the final atlas $\mathcal{A}$ can be modeled by the following function:

$$\left| \begin{array}{ll} \mathcal{A}' : I \rightarrow & \mathbb{R}^7 \\ \quad \mathbf{x} \mapsto & (d, a, \sigma_a, \theta, \sigma_\theta, \phi, \sigma_\phi)(\mathbf{x}) \end{array} \right. ,$$

which enables to store it in a simple way (as seven 3D gray-level images) and to easily recover any useful information it contains.

6 Atlas-guided vessel segmentation

Vascular atlases generated by the previously described method are essentially devoted to guidance of vessel segmentation algorithms. In this section, the proposed segmentation method uses such a cerebral vascular atlas. This atlas is used here to constrain mathematical morphology operators (gray-level hit-or-miss transform) for detection of vascular structures. In the first part of this section, background notions on hit-or-miss transform and its gray-level generalization are provided. These notions are necessary to understand and justify the segmentation method described in the second part of the section.

6.1 Theoretical background: Gray-level hit-or-miss transform

The hit-or-miss transform is a classical tool for extraction of templates from binary images. It uses a couple of structuring elements $(A, B) \in \mathcal{P}(\mathcal{E}) \times \mathcal{P}(\mathcal{E})$ where A (resp. B) has to fit the object (resp. the background). The binary hit-or-miss operation ($\otimes$)

can then be defined by:

$$X \otimes (A, B) = \{p \in \mathcal{E} \mid A_p \subseteq X, B_p \subseteq X^c\},$$

where $X \in \mathcal{P}(\mathcal{E})$ is a binary object of a given Euclidean or digital space (in our case, $\mathcal{E} \subset \mathbb{Z}^3$).

Any increasing operator can be extended to gray-level images by considering them as stacks of binary images. However the hit-or-miss transform, as previously defined, is not an increasing operation. Another definition ($\circledcirc$) has then been proposed in [54]:

$$X \circledcirc (A, B) = \{p \in \mathcal{E} \mid A_p \subseteq X \subseteq B_p\}.$$

The gray-level hit-or-miss operation can then be defined by:

$$F \circledcirc (A, B) = \bigvee \{i_{(p,t)} \mid A_{(p,t)} \leq F \leq B_{(p,t)}\},$$

where F is a gray-level function, $A, B : \mathcal{E} \to \overline{\mathbb{R}}$ are structuring functions ($A \leq B$) and $i_{(p,t)}$ is the impulse function defined by:

$$i_{(p,t)}(x) = \begin{cases} t & \text{if } x = p \\ -\infty & \text{if } x \neq p \end{cases}.$$

In [54], it has then been demonstrated that:

$$[F \circledcirc (A, B)](p) = \begin{cases} (F \ominus A)(p) & \text{if } (F \ominus A)(p) \geq (F \oplus B^*)(p) \\ -\infty & \text{otherwise} \end{cases}.$$

Choosing two structuring elements A_e and B_e, and two gray-levels a and b, with $a \geq b$, it becomes possible to define the gray-level structuring elements A and B by:

$$A(p) = \begin{cases} a & \text{if } p \in A_e \\ -\infty & \text{if } p \notin A_e \end{cases}, \text{ and } \quad B(p) = \begin{cases} b & \text{if } p \in B_e \\ +\infty & \text{if } p \notin B_e \end{cases},$$

and then obtain:

$$F \ominus A = (F \ominus A_e) - a, \text{ and } F \oplus B^* = (F \oplus \check{B}_e) - b,$$

and finally:

$$[F \oslash (A, B)](p) = \begin{cases} (F \ominus A_e)(p) - a & \text{if} (F \ominus A_e)(p) \geq (F \oplus \check{B}_e)(p) + a - b \\ -\infty & \text{otherwise} \end{cases}.$$

Using this definition is equivalent to compare, for each point, the minimum intensity a_{min} of all points within A_e and the maximum intensity b_{max} of all points within B_e. If $a_{min} \geq b_{max} + a - b$, then the point belongs to the transform.

6.2 Method

The proposed segmentation method is based on the use of the gray-level hit-or-miss transform. Another definition of this gray-level mathematical morphology operator [55] has already been used in [56] for the detection of the portal vein entry in liver CTA. A fixed-sized operator was then described to fit this precise anatomical structure. In this paper, we propose to use the gray-level hit-or-miss transform in an adaptive way, to carry out a segmentation of the whole cerebral arterial and venous trees.

6.2.1 Input and output

The method takes as input a PC MRA (p) of the whole head, composed of both phase (p_{pha}) and magnitude (p_{mag}) images (see Fig. 1), a vascular atlas ($\mathcal{A}$) generated by the method described in Section 5, and the reference PC MRA magnitude image (p^{ref}_{mag}) associated to the atlas. It provides as output a binary image p_{seg} of the arterial and venous trees.

6.2.2 Shape of the structuring elements

In order to fit the searched vascular structures, two kinds of structuring elements have to be determined. The element A, chosen for vessel modeling, is a discrete sphere of radius r_A, while the element B, chosen to model the neighboring background, is a set of 6 points sampled from a circle of radius r_B, having the same center than A and oriented according to angles (θ_B, ϕ_B). The choice of spheres instead of ellipsoids for vessel modeling is justified by their higher robustness in case of vessel tortuosity which may happen for many cerebral arteries. The use of points sampled from a circle instead of a whole discrete circle can allow a better detection of the background in case of vessel junctions or bifurcations, with a lower computation time. It has to be noticed that choosing (A, B) as being a discrete sphere and a sampled discrete circle does not only generate one couple of structuring elements

but a whole set of structuring elements of size and orientation depending on the radius and angular parameters (r_A, r_B, θ_B, ϕ_B). A subset of such structuring elements is illustrated in Fig. 5. Moreover, two supplementary intensity parameters a and b have to be added to these four shape parameters.

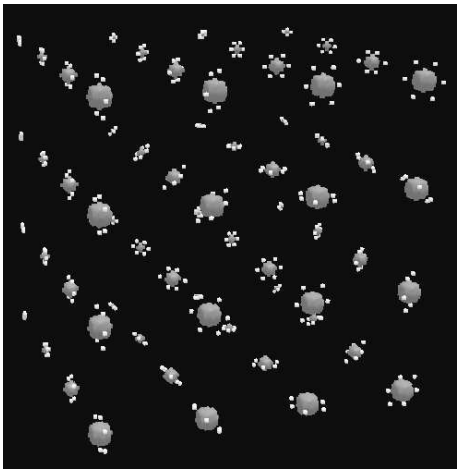

Fig. 5. Part of the family of the couple of structuring elements (A, B) used to carry out the gray-level hit-or-miss segmentation. The elements A (discrete spheres modeling the vessels) are represented in gray while the elements B (sampled discrete circles) are represented in white.

6.2.3 Use of the atlas

The immediate approach consisting in applying every couple of structuring elements in each point of the studied MRA (p_{pha}), to obtain the segmented image (p_{seg}):

$$p_{seg} = \{p \in p_{pha} \mid \exists (r_A, r_B, \theta_B, \phi_B, a, b), (p_{pha} \ominus A)(p) \geq (p_{pha} \oplus \check{B}) + a - b\},$$

leads to a prohibitive computational complexity. Indeed, for a 256^3 MRA, 5 distinct values for r_A (1 to 5 mm) and r_B (r_A + 1 mm to r_A + 5 mm), 5 angular positions for θ_B and ϕ_B, and 10 distinct values for $a - b$, this strategy requires to apply more than 10^{10} operators for one data. It is then necessary to reduce the algorithm complexity. This can be done by selecting, for each voxel assumed to belong to a vessel, a subset of structuring elements sufficiently small to allow an efficient computation time and sufficiently large to however correctly detect the vascular structures. Anatomical knowledge modeled by the vascular atlas $\mathcal{A}$ can be used to make this selection. Indeed, it provides a statistical estimation of vessel parameters (diameter and orientation) for each voxel. It is then an efficient tool to determine subsets of structuring elements adapted to every part of the processed image.

6.2.4 Algorithm

The first step of the segmentation method consists in applying a 3D deformation field on the vascular atlas $\mathcal{A}$ in order to obtain an atlas adapted to the considered MRA. This can be done by using the same registration algorithm as the one involved in the atlas generation process [52,53]. By registering p_{mag}^{ref} onto p_{mag}, a 3D deformation field is obtained, enabling to create a vascular atlas $\mathcal{A}_{reg}$ correctly fitting the cerebral structures of p.

The second step of the method is the determination of a set S of voxels assumed to contain the vascular structures. The voxels contained in S will then be the only ones to be processed by the gray-level hit-or-miss transform for vessel detection. This step is crucial for complexity reduction of the method. Indeed, brain vessels represent less than 3% of the image volume (generally containing more than 10^7 voxels). The set S is initialized to $\emptyset$. For each voxel $\mathbf{x}$ of p, $\mathbf{x}$ is added to S if and only if $\mathcal{A}_{reg}^{d}(\mathbf{x}) > 0$. This means that all points presenting a vascular density equal to 0 (*i.e.* all points where the probability to find a vessel is null, according to the atlas) will no longer be considered during the segmentation process. Eliminating such voxels enables to avoid processing the background or areas presenting no vessels (or no vessels which can be visualized by MRA) such as the cerebellum or the skull.

The third step consists in determining, for all $\mathbf{x} \in S$, a subset $S_{\mathbf{x}}$ of structuring elements (A, B) to be applied on the phase image p_{pha} at position $\mathbf{x}$. For each $\mathbf{x} \in S$, $S_{\mathbf{x}}$ is created by choosing elements (A, B) such as the radius of A (resp. the orientation of B) is a possible radius (resp. a possible orientation) according to $\mathcal{A}_{reg}$ (*i.e.* $r_A \in \mathcal{A}_{reg}^{t}(\mathbf{x})$ and $(\theta_B, \phi_B) \in \mathcal{A}_{reg}^{o}(\mathbf{x})$). A supplementary constraint is added for B which must be higher than the one of A and lower than twice it ($r_B \in]r_A, 2r_A]$). Since the structuring elements are discrete objects, only discrete diameters and orientations (orientations according to discrete lines) are considered. The determination of r_A (resp. of r_B) radii is done by selecting values of $\mathcal{A}_{reg}^{t}(\mathbf{x}) \cap \mathbb{N}$ (resp. of $]r_A, 2.r_A] \cap \mathbb{N}$). When $\mathcal{A}_{reg}^{t}(\mathbf{x}) \cap \mathbb{N} = \emptyset$ while $\mathcal{A}_{reg}^{t}(\mathbf{x}) \neq \emptyset$, the only selected value is chosen as being $\min\{n \in \mathbb{N} \mid n > \mathcal{A}_{reg}^{t}(\mathbf{x})\}$. In the same way, for all point $\mathbf{x} \in I$, the set $\mathcal{A}_{reg}^{o}(\mathbf{x})$ is discretized by intersection with $(\{\frac{k\pi}{n}\}_{k=0}^{n-1})^2$ for a chosen sampling value $n \in \mathbb{N}$. When $\mathcal{A}_{reg}^{o}(\mathbf{x}) \cap (\{\frac{k\pi}{n}\}_{k=0}^{n-1})^2 = \emptyset$ while $\mathcal{A}_{reg}^{o}(\mathbf{x}) \neq \emptyset$, the orientations are chosen in $\{\frac{k_\theta \pi}{n}, \frac{(k_\theta+1)\pi}{n}\} \times \{\frac{k_\phi \pi}{n}, \frac{(k_\phi+1)\pi}{n}\}$ such as $[\frac{k_\theta \pi}{n}, \frac{(k_\theta+1)\pi}{n}] \times [\frac{k_\phi \pi}{n}, \frac{(k_\phi+1)\pi}{n}] \supset \mathcal{A}_{reg}^{o}(\mathbf{x})$ (with $k_\theta, k_\phi \in \mathbb{N}$). It has to be noticed that a fixed low value has been chosen for $a-b$, enabling to detect vascular structures presenting a low contrast with the background.

The last step finally consists in applying the gray-level hit-or-miss transform on each candidate point using the subset of adapted structuring elements. Then, for each $\mathbf{x} \in S$, all operators $(A, B) \in S_{\mathbf{x}}$ are successively applied on $p_{pha}(\mathbf{x})$. If one of them matches a structure (*i.e.* if $(p_{pha} \ominus A)(\mathbf{x}) \geq (p_{pha} \oplus \check{B})(\mathbf{x}) + a - b$), the point $\mathbf{x}$ is added to the result image p_{seg}. In order to obtain a volumic object, for each point

x detected by a couple of structuring elements (A, B), a dilation by A_e is finally carried out in p_{seg} at the position **x** (if more than one operator $(A, B) \in S_{\mathbf{x}}$ matches a structure, the dilation is performed using the element A of highest radius).

7 Experiments and results

The validations and the result descriptions proposed in this section (atlas description and analysis, validations of vessel segmentations) have been carried out by an anatomist.

7.1 Implementation

The proposed methods have been implemented on the Medimax [3] software platform, using the ImLib3D [4] open source C++ library [57]. The computer used for validations was composed of a 2.8 GHz Pentium IV processor with 2 GB of memory.

The first step of the atlas generation process requires 20 minutes for automatic segmentation of each image of the database. The interactive correction time can vary according to the quality of this first segmentation. The validation and correction of a 18 image database can then require several hours. For each image of the database, the following quantitative analysis requires 5 minutes, while the second step of the atlas generation process is performed in 10 minutes, which represent the time required by the non-rigid registration method to superimpose two 3D PC MRA magnitude images with a millimetric resolution [5]. The data fusion required 15 minutes for a 18 image database. The average computation time for the segmentation method is 20 minutes to segment one PC MRA (10 minutes for non-rigid registration and 10 minutes for segmentation).

7.2 MRA database

The validations have been made on a 48 PC MRA database. A subset of 18 images has been used to create a vascular atlas, while the 30 remaining ones have been used to test the segmentation method. The MRA exams were performed on a 1

[3] Available at `http://www-ipb.u-strasbg.fr/gitim`.

[4] Available at `http://imlib3d.sourceforge.net`.

[5] Since non-rigid registration is independent from knowledge extraction, it could be possible to simultaneously carry out both steps on different computers, thus reducing the computation time.

Tesla whole-body scanner (Gyroscan NT/INTERA 1.0 T from Philips, gradient slope 75 T/m/s). The flow encoding sequence (T1FFE/PCA) uses a TR of 10 ms and a TE of 6.4 ms. The pool of patients was composed of males and females aged from 21 to 80, who did not present cerebral vascular pathologies. Sagittal slices of one of these images are illustrated in Fig. 1. The acquired images of dimensions varying from $256^2 \times 150$ to $256^2 \times 180$ voxels, were made of non-isotropic voxels of edges varying from 0.9 to 1.3 mm. The images have been processed to provide isotropic data.

7.3 Vascular atlas

The atlas generation method proposed in Section 5 has been tested on a 18 MRA database. The obtained vascular atlas is described and analyzed hereafter. It has been computed to fit a chosen reference PC MRA magnitude image (p_{mag}^{ref}), and then presents same properties as this image. It is then composed of $256 \times 229 \times 160$ voxels, each voxel being a cube of 1.13 mm edges. Parts of this atlas are illustrated in Fig. 6.

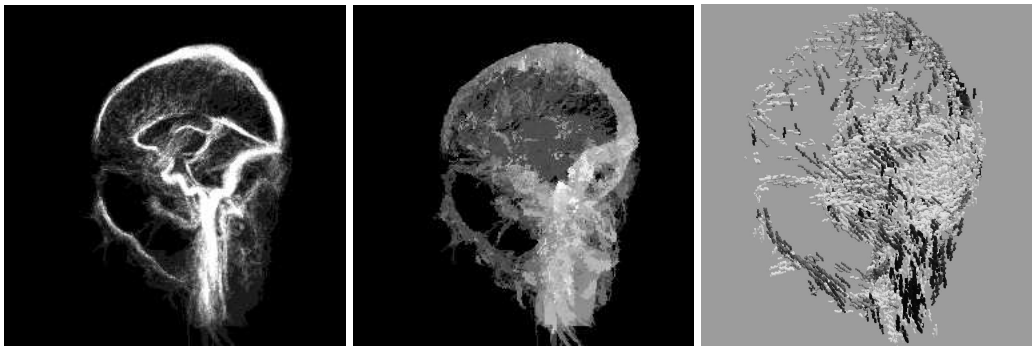

Fig. 6. Visualization of pieces of the processed atlas. Left: vascular density ($\mathcal{A}^d$), visualized as a maximum intensity projection of the sagittal slices; the brighter the region, the higher the probability to find a vessel. Middle: average vessel diameters (part a of $\mathcal{A}^t$), visualized as a maximum intensity projection of the sagittal slices; the brighter the region, the larger the vessels. Right: 3D visualization of a part of the orientation image ($\mathcal{A}^o$). Lines are oriented according to θ and ϕ; the gray level linearly depends on the θ value.

7.3.1 Vascular density

The vascular density ($\mathcal{A}^d$) represents the probability to find a vessel at a given position. A maximum intensity projection of this probability field is illustrated in the left part of Fig. 6. One can clearly observe invariant structures such as many veins and sinuses (superior sagittal sinus, straight sinus, transverse and sigmoid sinuses, jugular veins) but also arterial structures (carotid and pericallosal arteries). The invariance of these structures could enable to interpret a part of the vascular

density image as a classical graph. Other vessels appear as "vascular clouds", such as many arteries located in the medial part of the brain. Such vascular clouds do not constitute modeling errors. They can correspond to a single vessel whose position presents a high variability according to other brain or head structures. They can also represent the vasculature of areas where the number of branches vary between different patients. In both cases, these clouds provide information which is different from more conventional graph models, but remains coherent with respect to vascular density (homogeneous size and/or orientation fields are observed in most of them, emphasizing the fact that they really model the density of a vessel or set of vessels.) One can observe that vessels presenting less variable but more tortuous trajectories are modeled as quite homogeneous structures. An example can be observed in the left part of Fig. 6, where the internal carotids (under the polygon of Willis), despite their non linear trajectory, are not modeled by a "vascular cloud" but by a real vessel shape.

A more quantitative representation of these probabilities is proposed in Table 1. It has to be noticed that the vessels are localized in a very small part of the whole image. Indeed, less than 4% of the atlas is assumed to contain vessels sufficiently large to be visualized in MRA data. This property of the atlas, which is correctly correlated to the anatomical reality, is the one that enables to dramatically reduce the complexity of the atlas-guided segmentation proposed in Section 6.

Probability	# voxels	Ratio
$p = 0$	9 028 698	96.26%
$0 < p \leq 0.1$	209 718	2.23%
$0.1 < p \leq 0.2$	87 390	0.93%
$0.2 < p \leq 0.3$	27 031	0.29%
$0.3 < p \leq 0.4$	13 192	0.14%
$0.4 < p \leq 0.5$	7 092	0.08%
$0.5 < p$	6 719	0.07%
$p \neq 0$	351 142	3.74%
Total	9 379 840	100.00%

Table 1
Distribution of the probability (p) to find a vascular structure. First column: values of p; second and third columns: number and ratio of voxels $\mathbf{x}$ such as $\mathcal{A}^d(\mathbf{x}) = p$.

7.3.2 Vessel diameter

The generated atlas also provides information concerning the diameter of the different vessels. A maximum intensity projection of the diameter image of the atlas is

proposed in the middle part of Fig. 6. The biggest vessels are localized in the neck and in the venous parts (sinuses) while the positions corresponding to arterial structures present smaller sizes. This distribution of vessel diameters is summarized in Table 2. It has to be noticed that very few diameters lower than 1 mm are observed. This can be explained by the limitations of the MRA acquisition process which still does not enable to obtain submillimetric data.

Diameter (mm)	# voxels	Ratio
$0 < t \leq 1.0$	5 066	1.44%
$1.0 < t \leq 2.0$	80 282	22.87%
$2.0 < t \leq 3.0$	111 372	31.73%
$3.0 < t \leq 4.0$	80 139	22.84%
$4.0 < t \leq 5.0$	56 547	16.12%
$5.0 < t \leq 6.0$	14 411	4.11%
$6.0 < t$	3 121	0.89%
Total	350 938	100.00%

Table 2
Distribution of the average diameter of the vessels in the vascular part of the image (part presenting non zero values for $\mathcal{A}^d$). First column: average diameter (t); second and third columns: number and ratio of voxels $\mathbf{x}$ such as $a(\mathbf{x}) = t$.

7.3.3 Vessel orientation

The atlas finally provides information concerning the orientation of the cerebral vascular structures. A 3D visualization of the orientations for the left part of the atlas is illustrated in the right part of Fig. 6. The distribution of the orientations is summarized in Table 3.

One can observe that most of the voxels presenting a defined θ orientation have a quite horizontal one ($\theta \in [\pi/3, 2\pi/3[$). These voxels belong to cerebral parts of the atlas containing venous structures which are often oriented in a nearly horizontal plane (superior sagittal sinus, straight sinus). Most of these structures also present a ϕ orientation close to the sagittal plane which explains the high ratio of voxels such as $\phi \in [\pi/3, 2\pi/3[$. However, a higher amount of voxels presenting a vertical orientation ($\theta \in [0, \pi/6[\cup[5\pi/6, \pi[$) could have been expected. This can be explained by the fact that many vessels presenting a vertical orientation are located in the neck (carotid arteries, jugular veins). Indeed, the non-rigid registration used in this method, which is essentially devoted to brain registration, provides satisfactory results for cerebral structures, but less accurate ones for those located in the neck. Then the standard deviation values generally obtained in this area are not sufficiently low to define the orientation.

More generally, the amount of voxels presenting defined orientation could be significantly increased by no longer considering the absolute orientation of the vessels but their relative orientation according to adjacent non vascular structures. As an example, the superior sagittal sinus relative orientation according to the surface of the skull is quite invariant. The same property can be observed for many vascular and non vascular structures (straight sinus and superior frontier of the cerebellum, brain superficial veins and cortex). In order to be modeled, such properties would require a fusion between an atlas as the one presented here and non vascular atlases.

Orientation	θ		ϕ	
(rad.)	# voxels	Ratio	# voxels	Ratio
Undefined	253 978	72.33%	261 496	74.48%
$[0, \pi/6[$	3 540	1.01%	7 298	2.08%
$[\pi/6, \pi/3[$	14 931	4.25%	24 873	7.08%
$[\pi/3, \pi/2[$	31 174	8.88%	21 669	6.17%
$[\pi/2, 2\pi/3[$	27 679	7.88%	16 898	4.81%
$[2\pi/3, 5\pi/6[$	13 597	3.87%	14 685	4.18%
$[5\pi/6, \pi[$	6 243	1.78%	4 223	1.20%
Total	351 142	100.00%	351 142	100.00%

Table 3
Distribution of the orientation of the vessels in the vascular part of the image (part presenting non zero values for $\mathcal{A}^d$). First column: values of θ or ϕ; second and third (resp. fourth and fifth) columns: number and ratio of voxels presenting the current orientation according to θ (resp. ϕ).

Finally, this atlas enables to determine a set of invariant properties which seems to be sufficiently coherent according to the anatomical reality to be used for guidance of vessel segmentation processes such as the one analyzed hereafter. It has to be noticed that the purpose of this first atlas is to be used for vessel segmentation guidance, but not yet to describe in the most perfect way all cerebral vessels. The invariant properties that it model have been checked and validated by an anatomist. More systematic comparison of this atlas and other ones, created from larger databases will be the object of further works.

7.4 Vessel segmentation

The brain vessel segmentation method proposed in Section 6 has been tested on 30 PC MRA data, using the vascular atlas described in Subsection 7.3. An example

of vascular tree segmented by the method is illustrated in Fig. 7. The results have been quantitatively compared to segmentations obtained with a region-growing algorithm [49] and interactively corrected by an anatomist. In average, it has been observed that 77% of vascular structures are correctly and automatically segmented by the proposed method. The comparison also demonstrates that it generates 23% of false negatives but only 1% of false positives.

The false positive ratio is quite satisfactory since it proves that the method is robust when applied on images containing a high amount of noise and artifacts. Indeed, the segmentation algorithm is essentially based on shape and size of structuring elements, but not on threshold values. Then it is not sensitive to non-tubular high-intensity artifacts which are generally the main cause of false positives generally observed in segmented angiographic data.

Nevertheless, the proposed method still presents weaknesses concerning the false negative ratio. These false negatives can be divided into two categories. The first one correspond to segmentation errors caused by the non-rigid registration process. Indeed, it might happen that the registration presents inaccuracies in areas where non vascular cerebral structures can hardly be delineated. An example is the superior border of the cerebellum, where the frontier between cerebellum and both cerebral hemispheres is not easily visible. Registration inaccuracies in this region can make straight sinus segmentation a hard task. The second category of non segmented structures correspond to vascular regions presenting non circular sections (sinuses, vessel junctions and bifurcations). In such cases, it may happen that the spherical structuring elements used to perform the segmentation do not match the vessels. Moreover, even if they detect a non tubular vascular structure, the vessel reconstructed by dilating the segmented point by a sphere will be smaller than the real vessel.

Finally, it appears that the obtained results are still not fully perfect, as the false negative ratio remains high. However, they are quite promising since the method is not sensitive to intensity variations, noise, and artifacts, which are the main causes of segmentation errors in most vessel segmentation methods. This is an important property since PC MRA data generally present a low signal to noise ratio and often contain artifacts. Moreover, all of the known problems that are identified, and which can cause false negatives might be resolved in further works. Possible improvements are detailed in Subsection 8.2.

Fig. 7. Segmented vascular tree obtained with the proposed method. The gray-levels correspond to the radii of the structuring elements which permitted to segment the points.

8 Discussion

8.1 Possible uses of vascular atlases

The atlases that can be generated by the method proposed in this paper [6] are essentially devoted to segmentation purpose. Indeed, reliable a priori information concerning vessel position, diameter, and orientation can be useful for guidance of several kinds of methods. Concerning methods based on filtering or application of mathematical morphology operators, this knowledge can be used to reduce the computation time without altering the accuracy of the result, as proposed in Section 6. However, a priori information could also be used in order to improve the effi-

[6] The proposed atlas generation method, initially designed to process bimodal PC MRA data, has only been applied on such PC MRA images. Although it has not yet been proved that it can be applied to other kinds of data, it can reasonably be assumed that it may provide results of similar quality if applied on couples of bimodal images presenting similar properties. Such couples of images could be composed of T1 MRI/TOF MRA or T1 MRI/CTA. The two main supplementary difficulties could then consist in the necessity to initially register both images of each couple in a correct way (which is already done, by definition, for PC MRA) and in the difference of resolution between millimetric and submillimetric data if using CTA.

ciency of deformable model algorithms. This kind of methods generally requires an accurate initialization to provide correct results (an approximate initialization can lead to an erroneous segmentation). A priori information on position and size of the vessels could then allow to efficiently and automatically generate an initial model shape close to the structures to be segmented. These parameters could also be used to guide the model evolution, by integrating them in the energy function to minimize. Many other applications of vascular atlases for segmentation purpose could be cited, such as automatic initialization of vessel tracking algorithms, or guidance of region-growing methods. For such vessel segmentation guidance applications, it could be important to use atlases created from large image databases, in order to fuse a maximal amount of information to efficiently model the possible variations of vessel positions, sizes and orientations. As an example, for the segmentation method proposed in this paper, an atlas created from an insufficiently large database could lead to the non detection of vessels in brain regions erroneously considered as presenting a null vascular density (a 18 case atlas however seems to avoid such drawback, as observed during the validations on 30 images). The use of atlases for segmentation guidance, as the use of any kind of a priori knowledge, has to be considered with care.

The experiments (atlas generation and atlas-based segmentation) described in the previous section deal with healthy patients MRA. It can be assumed that the use of an atlas based on healthy people MRA is adapted to guide segmentation of MRA data without vascular pathologies (for surgery planning or functional analysis). A segmentation method based on such an atlas could however fail in segmenting severe aneurysms and stenoses (which respectively correspond to broadening and narrowing of vessels) since these pathological structures present properties differing from normal vessels. A way to enable the correct segmentation of MRA containing pathologies guided by an atlas made from MRA of healthy patients could consist in no longer considering the information provided by the vessel diameter field. Indeed, the main difference between normal vessels and pathological structures is linked to their size. However, efficient use of vascular atlases for segmentation of pathological structures would probably require to develop more complete or more sophisticated vascular atlases as it will be discussed in the next subsection.

Other kinds of applications than segmentation guidance may be considered. Assuming that the method is applied on a set of images not containing any cerebral pathologies, the resulting atlas, although not adapted to segment pathological structures, could be used as a reference for analyzing segmented MRA of non-healthy patients and detecting such structures. Since an atlas provides an estimation of the expected diameter for each main vessel of the brain, it could be a useful reference to help the clinicians to detect and quantify these pathological structures. Such an atlas could also be used for anatomical comparison, in order to determine the variability of the different vascular structures of the brain. This could lead to the creation of reliable and exhaustive descriptions of these structures, taking into account all their different configurations. Other applications such as creation of pathological

atlases, or atlases discriminating veins and arteries for labeling purpose, could also be considered.

8.2 Analysis and further works

The results obtained by application of both methods, and described in the previous section, are already promising, but could still be improved.

The vascular atlas generated from a database of 18 angiographic data enables to model knowledge on density and vessel size in a way being sufficiently accurate to correctly guide the proposed vessel segmentation process. The density field provides information on vessels position which seem to be satisfying with respect to the non vascular cerebral structures, while the vessel size fields are coherent with the diameters of the different venous and arterial structures which can be visualized in MRA images. However, size modeling is based on a Gaussian model and then gives, at each point, a set of possible sizes depending on the mean and standard deviation of diameter values observed in the database. This model could then be inaccurate in regions containing different vessels of very heterogeneous sizes. This may happen in very few cases in the neck where small arteries separate from larger ones, or at the confluence of straight and superior sagittal sinuses, where small anastomoses sometime replace larger vascular structures. Although such examples remain unusual, they would justify the development of alternative vessel size modeling strategies. Since the most frequent case leading to modeling inaccuracies correspond to the presence, in a same area, of several vessels presenting quite different sizes or orientations, an alternative solution could consist in detecting the presence of these different kinds of vessels at a same position, and to associate specific size and orientation Gaussian parameters to each of them. A labeling process of the vascular tree skeleton during the knowledge extraction step could enable such a preliminary detection. For each point of the atlas, it would then be necessary to no longer associate single mean and variance values, but sets of mean and variance ones. Information concerning vessel orientation also remains less informative than it could be. In the previous section, the main causes of these orientation inaccuracies have been identified. The first one is the use of non-rigid registration tools which are mainly devoted to brain structures, but still present less satisfactory results in other anatomical structures of the head. The development of ad hoc non-rigid registration devoted to the whole head should then constitute a first solution to this problem. The second problem is the use of absolute orientation in the modeling process. Cerebral vascular structures often present very precise orientation properties with respect to non vascular anatomical structures. It then seems necessary to develop, in further works, methods involving both vascular and non-vascular atlases for vessel property modeling.

Another solution to improve the efficiency of vascular atlases could consist in fus-

ing the different anatomical properties into a unified way instead of modeling them as independent fields. This could be done by creating atlases composed of adaptive subsets of possible geometrical shapes assumed to model the vessels. Such shapes could then gather information not only on size and orientation, but also on vessel cross-section form (which is a parameter not yet integrated in the current method). It has to be noticed that the creation of such atlases could provide an efficient way to solve the main problem of the proposed segmentation method. Indeed, most of the segmentation errors observed in the previous results are caused by the fixed shape of the used structuring elements. These atlases would allow an automatic generation of 3D structuring elements, the structure of which would evolve to fit the searched vascular structures. This could also provide a more reliable way to segment and detect pathological structures by also considering structuring elements corresponding to shapes and sizes of aneurysms and stenoses.

Further works will then focus on development of such an atlas generation method, but also on improvement of the existing one. Both methods will also be used to propose new mathematical morphology-based vessel segmentation methods as the one proposed in this paper. More generally, since the proposed results tend to prove that anatomical knowledge can be efficiently used in vessel segmentation strategies, further works will also consist in developing other kinds of methods based on this assumption, but not necessarily using the same modeling strategies.

Acknowledgments

The authors thank the PPF IRMC [7] (Plan Pluri-Formation Imagerie et Robotique Médicale et Chirurgicale) for its financial support. They also thank V. Noblet, M.-A. Jacob-Da Col, D. Chillet and C. Jahn, whose assistance largely contributed to this work.

References

[1] C. Dumoulin, H. Hart, Magnetic resonance angiography, Radiology 161 (1986) 717–720.

[2] F. Wehrli, A. Shimakawa, G. Gullberg, J. McFall, Time of flight MR flow imaging: Selective saturation recovery with gradient refocusing, Radiology 160 (1986) 781–785.

[3] C. Dumoulin, S. Souza, M. Walker, W. Wagle, Three-dimensional phase contrast angiography, Magnetic Resonance in Medicine 9 (1989) 139–149.

[7] http://irmc.u-strasbg.fr

[4] K. Bühler, P. Felkel, A. La Cruz, Geometric methods for vessel visualization and quantification - A survey, Technical report VRVis-2002-035, VRVis Center (2002).

[5] P. Felkel, R. Wegenkittl, A. Kanitsar, Vessel tracking in peripheral CTA datasets - An overview, in: Spring Conference on Computer Graphics - SCCG'01, 2001, pp. 232–239.

[6] C. Kirbas, F. Quek, A review of vessel extraction techniques and algorithms, ACM Computing Surveys 36 (2004) 81–121.

[7] J. Suri, K. Liu, L. Reden, S. Laxminarayan, A review on MR vascular image processing: Skeleton versus nonskeleton approaches: Part II, IEEE Transactions on Information Technology in Biomedicine 6 (2002) 338–350.

[8] G. Marchal, D. Vandermeulen, H. Bosmans, D. Delaere, P. Suetens, A. Baert, A three-dimensional line filter for improved visualization of MRA, Supplement to Radiology 177 (1990) 259.

[9] G. Gerig, O. Kübler, R. Kikinis, F. Jolesz, Nonlinear anisotropic filtering of MRI data, IEEE Transactions on Medical Imaging 11 (1992) 221–232.

[10] H. Chen, J. Hale, An algorithm for MR angiography image enhancement, Magnetic Resonance in Medicine 33 (1995) 534–540.

[11] Y. Du, D. Parker, Vessel enhancement filtering in three-dimensional angiograms using long-range signal correlation, Journal of Magnetic Resonance Imaging 7 (1997) 447–450.

[12] M. Orkisz, C. Bresson, I. Magnin, O. Champin, P. Douek, Improved vessel visualization in MR angiography by nonlinear anisotropic filtering, Magnetic Resonance in Medicine 37 (1997) 914–919.

[13] C.-F. Westin, L. Wigström, T. Loock, L. Sjöqvist, R. Kikinis, H. Knutsson, Three-dimensional adaptive filtering in magnetic resonance angiography, Journal of Magnetic Resonance Imaging 14 (2001) 63–71.

[14] Y. Sun, D. Parker, Small vessel enhancement in MRA images using local maximum mean processing, IEEE Transactions on Image Processing 10 (2001) 1687–1699.

[15] G. Gerig, T. Koller, G. Székely, C. Brechbühler, O. Kübler, Symbolic description of 3-D structures applied to cerebral vessel tree obtained from MR angiography volume data, in: Information Processing in Medical Imaging - IPMI'93, Vol. 687 of Lecture Notes in Computer Science, 1993, pp. 94–111.

[16] N. Passat, C. Ronse, J. Baruthio, J.-P. Armspach, J. Foucher, Using watershed and multimodal data for vessel segmentation: Application to the superior sagittal sinus, in: Mathematical Morphology: 40 years on - Proceedings of the 7th International Symposium on Mathematical Morphology, Vol. 30 of Computational Imaging and Vision, 2005, pp. 419–428.

[17] S. Kobashi, Y. Hata, Y. Tokimoto, M. Ishikawa, Automatic segmentation of blood vessels from MR angiography volume data by using fuzzy logic technique, in: Medical Imaging: Image Processing 1999, Vol. 3661 of SPIE Proceedings, 1999, pp. 968–976.

[18] P. Yim, P. Choyke, R. Summers, Gray-scale skeletonization of small vessels in magnetic resonance angiography, IEEE Transactions on Medical Imaging 19 (2000) 568–576.

[19] H. Cline, C. Dumoulin, W. Lorensen, S. Souza, W. Adams, Volume rendering and connectivity algorithms for MR angiography, Magnetic Resonance in Medicine 18 (1991) 384–394.

[20] U. Klose, D. Petersen, J. Martos, Tracking of cerebral vessels in MR angiography after highpass filtering, Magnetic Resonance Imaging 13 (1995) 45–51.

[21] W. Lin, E. Haacke, T. Masaryk, A. Smith, Automated local maximum-intensity projection with three dimensional vessel tracking, Journal of Magnetic Resonance Imaging 2 (1992) 519–526.

[22] X. Hu, N. Alperin, D. Levin, K. Tan, M. Mengeot, Visualization of MR angiographic data with segmentation and volume-rendering techniques, Journal of Magnetic Resonance Imaging 1 (1992) 539–546.

[23] D. Saloner, W. Hanson, J. Tsuruda, R. van Tyen, C. Anderson, R. Lee, Application of connected-voxel algorithm to MR angiographic data, Journal of Magnetic Resonance Imaging 1 (1991) 423–430.

[24] O. Wink, W. Niessen, M. Viergever, Fast delineation and visualization of vessels in 3D angiographic images, IEEE Transactions on Medical Imaging 19 (2000) 337–346.

[25] H. Ehricke, K. Donner, W. Koller, W. Strasser, Visualization of vasculature from volume data, Computer & Graphics 18 (1994) 395–406.

[26] N. Flasque, M. Desvignes, J. Constans, M. Revenu, Acquisition, segmentation and tracking of the cerebral vascular tree on 3D magnetic resonance angiography images, Medical Image Analysis 5 (2001) 173–183.

[27] C. Lorenz, I.-C. Carlsen, T. Buzug, C. Fassnacht, J. Weese, Multi-scale line segmentation with automatic estimation of width, contrast and tangential direction in 2D and 3D medical images, in: Computer Vision, Virtual Reality and Robotics in Medicine and Medical Robotics and Computer-Assisted Surgery - CVRMed-MRCAS'97, Vol. 1205 of Lecture Notes in Computer Science, 1997, pp. 233–242.

[28] Y. Sato, S. Nakajima, N. Shiraga, H. Atsumi, S. Yoshida, T. Koller, G. Gerig, R. Kikinis, Three-dimensional multi-scale line filter for segmentation and visualization of curvilinear structures in medical images, Medical Image Analysis 2 (1998) 143–168.

[29] K. Krissian, G. Malandain, N. Ayache, R. Vaillant, Y. Trousset, Model-based detection of tubular structures in 3D images, Computer Vision and Image Understanding 80 (2000) 130–171.

[30] V. Prinet, O. Monga, S. Ge, C. Xie, S. Ma, Thin network extraction in 3D images: Application to medical angiograms, in: International Conference on Pattern Recognition - ICPR'96, Vol. 3, 1996, pp. 386–390.

[31] S. Aylward, E. Bullit, Initialization, noise, singularities, and scale in height ridge traversal for tubular object centerline extraction, IEEE Transactions on Medical Imaging 21 (2002) 61–75.

[32] E. Bullitt, S. Aylward, K. Smith, S. Mukherji, M. Jiroutek, K. Muller, Symbolic description of intracerebral vessels segmented from magnetic resonance angiograms and evaluation by comparison with X-ray angiograms, Medical Image Analysis 5 (2001) 157–169.

[33] L. Lorigo, O. Faugeras, W. Grimson, R. Keriven, R. Kikinis, A. Nabavi, C.-F. Westin, CURVES: Curve evolution for vessel segmentation, Medical Image Analysis 5 (2001) 195–206.

[34] P. Yim, J. Cebral, R. Mullick, P. Choyke, Vessel surface reconstruction with a tubular deformable model, IEEE Transactions on Medical Imaging 20 (2001) 1411–1421.

[35] P. Yim, G. Boudewijn, C. Vasbiner, V. Ho, P. Choyke, Isosurfaces as deformable models for magnetic resonance angiography, IEEE Transactions on Medical Imaging 22 (2003) 875–881.

[36] A. Frangi, W. Niessen, R. Hoogeveen, T. van Walsum, M. Viergever, Model-based quantitation of 3-D magnetic resonance angiographic images, IEEE Transactions on Medical Imaging 18 (1999) 946–956.

[37] A. Chung, J. Noble, P. Summers, Fusing speed and phase information for vascular segmentation of phase contrast MR angiograms, Medical Image Analysis 6 (2002) 109–128.

[38] M. Sabry Hassouna, A. Farag, S. Hushek, T. Moriarty, Statistical-based approach for extracting 3D blood vessels from TOF-MRA data, in: Medical Image Computing and Computer-Assisted Intervention - MICCAI'03, Vol. 2878 of Lecture Notes in Computer Science, 2003, pp. 680–687.

[39] D. Wilson, J. Noble, An adaptive segmentation algorithm for time-of-flight MRA data, IEEE Transactions on Medical Imaging 18 (1999) 938–945.

[40] B. Avants, J. Williams, An adaptive minimal path generation technique for vessel tracking in CTA/CE-MRA volume images, in: Medical Image Computing and Computer-Assisted Intervention - MICCAI'00, Vol. 1935 of Lecture Notes in Computer Science, 2000, pp. 707–716.

[41] S. Kobashi, N. Kamiura, Y. Hata, F. Miyawaki, Volume-quantization-based neural network approach to 3D MR angiography image segmentation, Image and Vision Computing 19 (2001) 185–193.

[42] C. Zahlten, H. Jürgens, C. Evertsz, R. Leppek, H.-O. Peitgen, K. Klose, Portal vein reconstruction based on topology, European Journal of Radiology 19 (1995) 96–100.

[43] P. Dokládal, C. Lohou, L. Perroton, G. Bertrand, Liver blood vessels extraction by a 3-D topological approach, in: Medical Image Computing and Computer-Assisted Intervention - MICCAI'99, Vol. 1679 of Lecture Notes in Computer Science, 1999, pp. 98–105.

[44] A. Sanderson, D. Parker, T. Henderson, Simultaneous segmentation of MR and X-ray angiograms for visualization of cerebral vascular anatomy, in: International Conference on Volume Image Processing VIP'93, 1993, pp. 11–14.

[45] I. Bloch, C. Pellot, F. Sureda, A. Herment, 3D reconstruction of blood vessels by multi-modality data fusion using fuzzy and Markovian modelling, in: Computer Vision, Virtual Reality and Robotics in Medicine - CVRMed'95, Vol. 905 of Lecture Notes in Computer Science, 1995, pp. 392–398.

[46] O. Musse, F. Heitz, J.-P. Armspach, Fast deformable matching of 3D images over multiscale nested subspaces. Application to atlas-based MRI segmentation, Pattern Recognition 36 (2003) 1881–1899.

[47] D. Chillet, J. Jomier, D. Cool, S. Aylward, Vascular atlas formation using a vessel-to-image affine registration method, in: Medical Image Computing and Computer-Assisted Intervention - MICCAI'03, Vol. 2878 of Lecture Notes in Computer Science, 2003, pp. 335–342.

[48] D. Cool, D. Chillet, J. Kim, S. Aylward, Tissue-based affine registration of brain images to form a vascular density atlas, in: Medical Image Computing and Computer-Assisted Intervention - MICCAI'03, Vol. 2879 of Lecture Notes in Computer Science, 2003, pp. 9–15.

[49] N. Passat, C. Ronse, J. Baruthio, J.-P. Armspach, C. Maillot, C. Jahn, Region-growing segmentation of brain vessels: An atlas-based automatic approach, Journal of Magnetic Resonance Imaging 21 (2005) 715–725.

[50] D. Chillet, N. Passat, M.-A. Jacob-Da Col, J. Baruthio, Thickness estimation of discrete tree-like tubular objects: Application to vessel quantification, in: Scandinavian Conference on Image Analysis - SCIA'05, 14th Scandinavian Conference, Proceedings, Vol. 3540 of Lecture Notes in Computer Science, 2005, pp. 263–271.

[51] G. Bertrand, A Boolean characterization of three-dimensional simple points, Pattern Recognition Letters 17 (1996) 115–124.

[52] V. Noblet, C. Heinrich, F. Heitz, J.-P. Armspach, A topology preserving non-rigid registration method using a symmetric similarity function - Application to 3-D brain images, in: European Conference on Computer Vision - ECCV'04, Vol. 3023 of Lecture Notes in Computer Science, 2004, pp. 546–557.

[53] V. Noblet, C. Heinrich, F. Heitz, J.-P. Armspach, 3D deformable image registration: A topology preservation scheme based on hierarchical deformation models and interval analysis optimization, IEEE Transactions on Image Processing 14 (5) (2005) 553–566.

[54] C. Ronse, A lattice-theoretical morphological view on template extraction in images, Journal of Visual Communication & Image Representation 7 (1996) 273–295.

[55] P. Soille, Advances in the analysis of topographic features on discrete images, in: Discrete Geometry for Computer Imagery - DGCI'02, Vol. 2301 of Lecture Notes in Computer Science, 2002, pp. 176–186.

[56] B. Naegel, C. Ronse, L. Soler, Using grey scale hit-or-miss transform for segmenting the portal network of the liver, in: Mathematical Morphology: 40 years on - Proceedings of the 7th International Symposium on Mathematical Morphology, Vol. 30 of Computational Imaging and Vision, 2005, pp. 429–437.

[57] M. Bosc, T. Vik, J.-P. Armspach, F. Heitz, ImLib3D: An efficient, open source, medical image processing framework in C++, in: Medical Image Computing and Computer-Assisted Intervention - MICCAI'03, Vol. 2879 of Lecture Notes in Computer Science, 2003, pp. 981–982.